Dynamic Evolution of Topological Defects around Drops and Bubbles Rising in a Nematic Liquid Crystal

Siddharth Khullar,[1] Chunfeng Zhou,[1] and James J. Feng[1,2,*]

[1]Department of Chemical and Biological Engineering, University of British Columbia, Vancouver, BC V6T 1Z3, Canada
[2]Department of Mathematics, University of British Columbia, Vancouver, BC V6T 1Z2, Canada

(Received 29 June 2007; published 7 December 2007)

We report observations of topological defects around drops and bubbles that rise through a vertically aligned nematic liquid crystal. We provide direct evidence for downstream convection of the Saturn-ring defect and its transformation to a hyperbolic point defect. The point defect is convected further in the wake of the drop or bubble as the rising velocity increases. In equilibrium, both defect configurations may persist for long times in the narrow cell. But the point defect sometimes spontaneously opens into a Saturn ring, indicating the latter as the globally stable configuration in the presence of tight wall confinement.

DOI: 10.1103/PhysRevLett.99.237802 PACS numbers: 61.30.Jf, 47.55.D−, 47.57.Lj

Liquid crystal dispersions, with droplets of an isotropic fluid suspended in a nematic medium, have gained significant attention for their novelty and electro-optic applications [1,2]. Topological defects and distortions generate elastic forces that mediate the interaction among the droplets [3]. Therefore, the study of defect dynamics in such systems is of considerable interest. This Letter reports experimental observations of flow effects on defects surrounding moving droplets and bubbles with homeotropic anchoring. In particular, we seek to resolve a contradiction in the literature about the convection of defects, and to provide direct evidence for flow-induced and spontaneous transitions between the defect configurations.

When a particle or droplet is placed in a nematic liquid crystal host, it enforces a surface molecular alignment that distorts the bulk orientation field around it [4]. Typically a topological defect is generated in the neighborhood of the inclusion. With planar anchoring on the interface, surface defects known as ''boojums'' appear on the poles of the particle [1]. This configuration seems to be extremely stable and will not be considered further in this Letter. With homeotropic anchoring, either a satellite point defect [1] or a Saturn-ring line defect [5,6] appears depending on initial conditions and the ratio $A = Wa/K$, where W is the anchoring constant, a is the radius of the particle, and K is the bulk elastic constant. The ring defect prevails for small A while the point defect does for large A [4,7,8]. The defect configuration may be manipulated by applying an external electric or magnetic field; it turns a point defect into a ring defect and vice versa [3,4,9].

The effect of a *flow* field on the defects has received far less attention. Motion and flow are involved in various dynamic processes in nematic dispersions, e.g., the self-assembly of droplets [1], and a thorough understanding of the hydrodynamic effects on defect evolution will be valuable. So far, there have been several computational studies. Stark and Ventzki [10] predicted that the flow around a particle will move a satellite point defect *upstream*. This was later contradicted by Yoneya *et al.* [11]. Since the defect is not a physical entity, its apparent ''convection'' reflects rearrangement of the orientational field rather than flow of materials. Thus, it is not intuitively obvious which prediction is correct. More recently, simulations by Zhou *et al.* [12] suggested that a defect ring around a rising drop convects downstream, and may be transformed into a point defect in the wake. The objective of the present study is to clarify this picture using direct experimental observations.

We observe the rise of bubbles and droplets in a vertical flow cell made from two microscope glass slides (7.5 cm × 5 cm) separated by a gap between 100 and 500 μm that is controlled by polyester spacers. The cell is filled with the liquid crystal 5CB (98% purity, Aldrich, density 1.008 g/cm^3), which is nematic within the temperature range of 22 °C to 35 °C. Most experiments are at a room temperature of 23 °C. The inner surface of the slides is coated with a thin layer of PVA (above 99% purity, Aldrich), which is then rubbed mechanically to create planar anchoring in the vertical direction. Air bubbles are injected into the nematic-filled cell via a microcapillary in conjunction with a pneumatic ''picopump'' (PV820, World Precision Instruments). Oil droplets (PDMS-RT5, Cannon Instrument, density 0.912 g/cm^3) are suspended in the nematic in a beaker and the suspension is then transferred into the cell. The diameter of the generated bubbles and drops ranges from 15 to 250 μm. In all the experiments, the bubbles and drops never visually deviate from the spherical shape. The following material parameters will be used in analyzing the results: bulk elastic constant $K = 10^{-11}$ N [13], anchoring energy $W = 10^{-5}$ N/m for the 5CB/air interface [14], and $W = 6 \times 10^{-6}$ N/m for the 5CB/PDMS interface [15], viscosity $\eta = 7.65 \times 10^{-2}$ Pa s [16].

For observations, we use an inverted polarizing microscope (Olympus IX-51) that lies on an optical table so the light path goes horizontally through the thickness of the cell. The first polarizer is along the vertical direction and the second horizontal. To capture the rising bubbles and drops, the cell is mounted on a motion control system. For

 © 2007 The American Physical Society

more quantitative examination of the molecular orientation, we employ the universally compensated polarizing technique (Abrio by CRI, Inc.) to map out the director field near nematic-isotropic interfaces [17,18]. Using Abrio and crossed polarizers, we have confirmed that the planar wall anchoring is uniformly vertical and the anchoring on the surface of air bubbles and oil droplets is homeotropic, as expected [19,20].

To observe *static defects* as a baseline, we use a wedge-shaped cell having a thinner gap at the top than the bottom to bring rising drops and bubbles to a stop. Both the Saturn-ring and satellite point defects have been observed in equilibrium, each apparently stable as it persists for hours. The ring configuration is apparent in Fig. 1(a). Figure 1(b), however, shows two bright lobes separated by a dark line in the middle. Using regularized Frank elasticity [12,21], we have computed the equilibrium director field surrounding a point defect as well as the transmitted light intensity if such a director field is viewed between crossed polarizers. The resulting pattern in Fig. 1(c) bears a close resemblance to the observed patterns, with the point defect close to the tip of the bright lobes. This confirms that Fig. 1(b) indeed shows a hyperbolic point defect, and the bright lobes are created by director orientation that is roughly midway between the two polarizers. Director maps generated by Abrio are consistent with the director field in Fig. 1(c). The distance between the point defect and the center of the drop or bubble, r_d, ranges from $1.14a$ to $1.25a$ among all bubbles and drops tested. The radius of the Saturn ring varies between $1.05a$ and $1.16a$. These are in close agreement with prior computations and observations [7].

For the oil drops in Fig. 1, $a \sim 30\ \mu$m and $A = Wa/K \sim 18$. For a freestanding particle of this size, prior calculations have shown the Saturn ring to be either metastable [7,22] or absolutely unstable [4], and experiments have only observed the point defect. However, wall confinement is known to stabilize the Saturn ring on particles as large as 50 μm in radius [6,13,23]. Evidently, the same mechanism is responsible for the Saturn ring in Fig. 1(a).

Occasionally, a point defect spontaneously opens up into a ring that expands and moves towards the bubble's equatorial plane, eventually becoming a Saturn ring (Fig. 2). The point-to-ring transition occurs rather sporadically, sometimes within a few minutes of the stoppage of the drop, sometimes after several hours. This may be a fluctuation-induced transition from one locally stable configuration to the other, suggesting the Saturn ring as the global energy minimizer under wall confinement in our wedged cell. This is also confirmed by heating the cell past the nematic-isotropic transition. Upon cooling back into the nematic state, the ring defect always appears. Note that Gu and Abbott [6] observed what appeared to be spontaneous ring-to-point transformations. Their surface-treated solid particles probably had stronger anchoring that favored the point defect.

By inverting the wedged cell containing a stationary drop bearing a Saturn ring, we study the evolution of the Saturn ring as the drop rises (Fig. 3). For the initial period, the rise velocity v is low and the ring stays at the drop's equator [3(a)]. Later the ring shifts downstream while v increases [3(b)]. The central part of the ring moves more slowly than the parts near the edge of the drop in the image, owing to the hindrance by the cell walls. Figures 3(c)–3(f) depict a relatively rapid transient wherein the ring is pushed further downstream and swept off the drop into a point defect in the near wake [3(f)]. Meanwhile v reaches a maximum and then declines toward a "terminal velocity." For the rest of the drop's rise, the point defect remains stable with no further convection downstream.

The apparent "convection" of defects reflects the rearrangement of the director field $\mathbf{n}(\mathbf{r})$ by viscous and elastic torques. Rotation of $\mathbf{n}$ due to the viscous torque (or flow) is on the time scale of the rising bubble, which is on the order of hours (cf. Fig. 3). The elastic time scale, on the other hand, is $\eta a^2/K \approx 5$ s for the oil drop with $a = 25.2\ \mu$m. Therefore, except for the fast transient during the shedding of the ring [Figs. 3(d)–3(f)], the process is *quasistatic* as far as the director field is concerned.

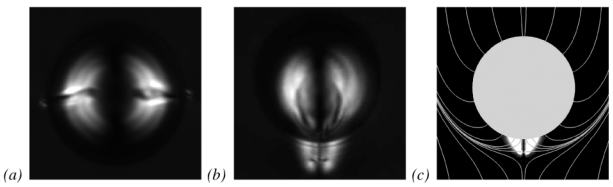

FIG. 1. Static defects surrounding oil drops viewed through crossed polarizers. (a) Saturn-ring defect (drop radius $a = 30.2\ \mu$m), (b) point defect ($a = 21.8\ \mu$m), (c) computed director field and light intensity graph for a point defect.

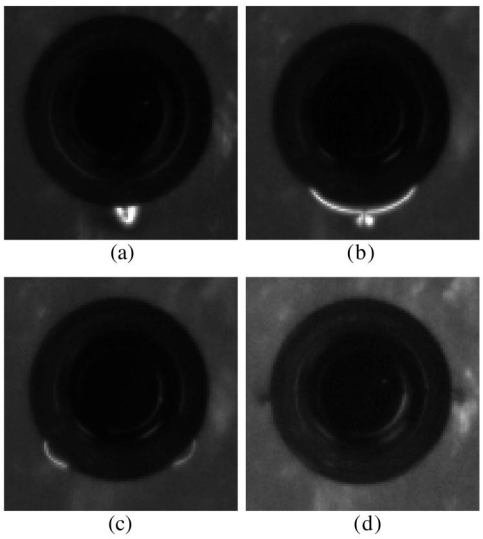

FIG. 2. Spontaneous point-to-ring transformation around a stationary bubble of radius $a = 100\ \mu$m. The images are taken through crossed polarizers, and (a) shows the characteristic birefringence pattern for the point defect [cf. Fig. 1(c)]. (a) $t = 0$ s, (b) $t = 217$ s, (c) $t = 281$ s, (d) $t = 428$ s.

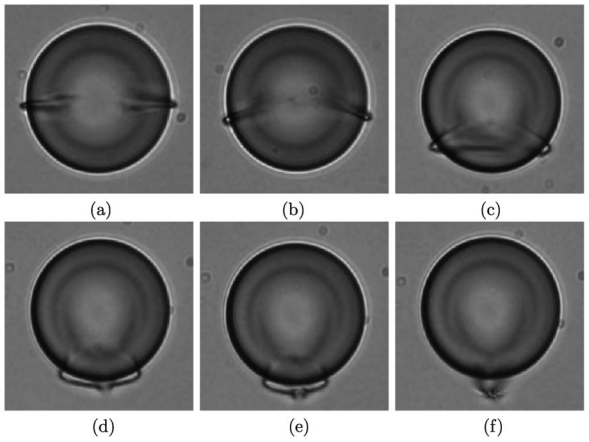

FIG. 3. Flow-induced ring-to-point transformation around a rising oil drop, $a = 25.2\ \mu$m. The time since the start of the rise and the instantaneous drop velocity for each frame are (a) 1074 s, 0.35 μm/s, (b) 9323 s, 0.87 μm/s, (c) 11 425 s, 1.05 μm/s, (d) 11 444 s, 1.27 μm/s, (e) 11 446 s, 1.29 μm/s, (f) 11 449 s, 1.08 μm/s. The images are taken with a single polarizer to clearly show the outline of the drop and defects, and the final frame corresponds to the two-lobed birefringence pattern for the point defect.

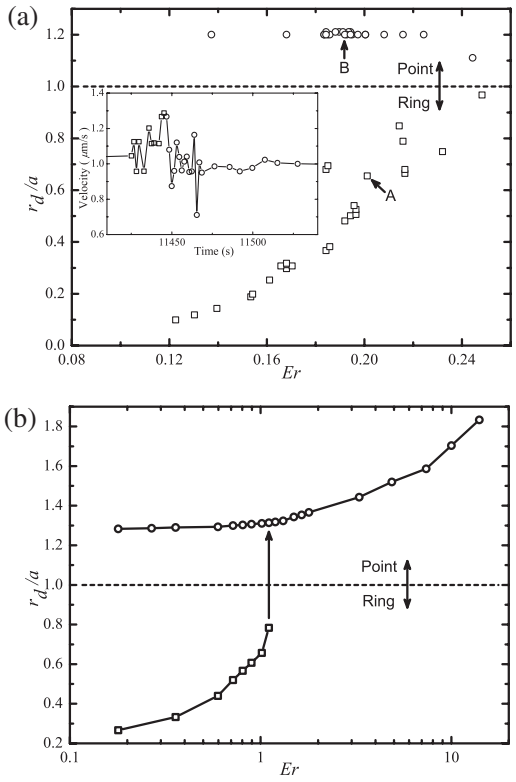

FIG. 4. (a) Position of the ring or point defect as a function of the Ericksen number Er for the oil drop of Fig. 3. For the Saturn ring (squares), r_d is the vertical distance between the drop center and the edge of the ring. For the satellite point defect (circles), r_d is the distance from the drop center. $A = 15.1$. The inset shows the velocity overshoot that coincides with the ring-to-point transition. Points A and B correspond to the first and last data points in the inset. (b) Numerical prediction of steady-state defect positions for $A = 30$, after Fig. 7 of Ref. [12], ©Cambridge University Press, reprinted with permission.

Besides, the motion is essentially inertialess (Reynolds number Re $\sim 10^{-6}$), and the variation of v simply reflects the ''drag coefficient'' changing with the surrounding director field. We have plotted the position of the ring or point defect as a function of the instantaneous drop velocity v, nondimensionalized as the Ericksen number $\mathrm{Er} = \eta v a/K$, in Fig. 4(a). The initial increase of r_d with Er corresponds to the downstream convection of the ring defect while the drop steadily accelerates. As Er approaches a critical value $\mathrm{Er}^c \approx 0.25$, the ring is quickly pushed to the downstream pole with $r_d \to a$; this is where the ring turns into a point defect. At this moment, the drop velocity drops suddenly (see inset), causing Er to decrease in time and generating the U-turn in the data. Meanwhile, the point defect shifts slowly downstream. Eventually, the drop and defect reach a steady state with $\mathrm{Er} \approx 0.19$ and $r_d \approx 1.2a$, indicated by point B. The two outlying circles farthest to the left correspond to the lowest velocity readings in the noisy overshoot. Therefore, for $0.19 \lesssim \mathrm{Er} \lesssim 0.25$, both the Saturn-ring and the point defect are stable solutions in our confined cell.

The convection of the ring defect and its transformation into a point defect agree qualitatively with recent computations of Zhou *et al.* [12]. The numerically predicted $r_d(\mathrm{Er})$ curves for steady-state flow are reproduced as Fig. 4(b). First, the experimental data follow the trend predicted numerically, but at considerably lower Er values. The critical value for ring-to-point transformation, $\mathrm{Er}^c \approx 0.25$, is below the predicted $\mathrm{Er}^c \approx 1$. Second, Zhou *et al.* predict the coexistence of the two defect configurations for $\mathrm{Er} < \mathrm{Er}^c$, which is also borne out by the data. For $\mathrm{Er} > \mathrm{Er}^c$, only the point defect is stable. The oil drops cannot access higher Er and that branch of the numerical curve will be discussed below. Note also that the fast transient in Figs. 3(d)–3(f) suggests that these intermediate configurations are not stable steady solutions, in accordance with the jump in Fig. 4(b). Finally, the overshoot of the drop velocity during the ring-to-point transformation has also been predicted. The coupling between the rise velocity and defect conformation has been explained via the anisotropic viscosity of the nematic [12].

We have to add two caveats on the above comparison. Our oil drop is confined between two walls imposing planar anchoring, whereas the computation is in an essentially unbounded domain. As mentioned before, the confinement has a strong stabilizing effect on the Saturn ring, similar to weakening the anchoring on the drop or reducing its diameter. Besides, the computation predicts the ring defect to persist to larger particle sizes than experimentally observed [1]. Thus, the quantitative discrepancy between the two is no surprise. In fact, the degree of agreement is rather astonishing given these complications.

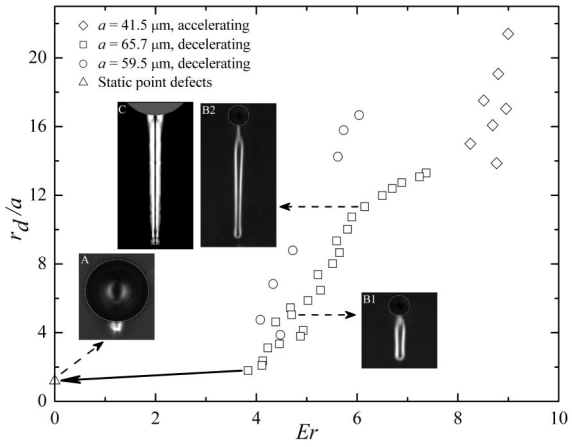

FIG. 5. Position of the point defect as a function of the instantaneous Ericksen number for accelerating and decelerating bubbles. Insets B1 and B2 show the bright birefringent loops with the point defect at the bottom, and C shows a computed birefringent pattern roughly corresponding to B2. The solid arrow indicates the final stabilization of the point defect to its equilibrium position, depicted in inset A.

In another series of experiments, we inject air bubbles instead of oil drops to achieve a higher rise velocity v. It is now more difficult to capture the initial ring-to-point transition because of the bubble's high velocity. Rather we will focus on the later stage of the bubble's rise. Once the point defect is formed, it is convected farther downstream in the wake. This is accompanied by a steady increase in v, with defect and bubble motion again being coupled. Through crossed polarizers, the point defect sits at the tip of a bright loop hanging from the bubble (insets B1 and B2 in Fig. 5), which is the bright lobes of Fig. 1(b) elongated up to $20a$ at the highest bubble speed. As the bubble reaches the narrower top of the wedged cell, it decelerates and the loop retracts with the point defect moving toward the bubble. It reverts to the relatively broad bright lobes as the bubble comes to a stop. The point defect may remain indefinitely but sometimes opens into a Saturn ring as illustrated in Fig. 2.

For bubble radius on the order of 60 μm, the elastic relaxation time is $\eta a^2/K \sim 28$ s. The entire rise takes some 200 s, and cannot be considered quasistatic. This implies that the defect configuration at any particular time is undergoing relaxation and is dependent on the history up to that point, and there is no one-to-one correlation between r_d and the instantaneous v or Er. Nevertheless, we have collected r_d data in Fig. 5. First, the scatter among different runs reflects the fact that transient effects due to elastic relaxation and history are at play. Second, the positive slope of the data, in both the accelerating and decelerating stages, is consistent with the steady-state computations of Zhou *et al.* [12] in Fig. 4(b), although the experimental r_d values are much higher than the computed ones for the same Er. In particular, the close proximity of the cell walls may have contributed to the elongated loop.

This study represents the first direct observation of dynamic evolution of defects near moving droplets or bubbles. The significance of the results is twofold. First, the experiment clarifies the picture suggested by prior computations. In particular, it settles the controversy on the direction of convection of defects, and provides direct evidence for flow-induced ring-to-point transformation. Second, insomuch as defects mediate the interaction among particulates in nematic media, the insights on defect evolution are useful for understanding pattern formation in flowing nematic colloids and dispersions. Moreover, the flow field may be used as a means to manipulate defect location and configuration near isotropic-nematic interfaces, much as electric and magnetic fields have been in the past.

We thank P. T. Mather, J. M. Gosline, and R. E. Shadwick for discussions on microscopic imaging, and T. I. Burghelea for help with the motion control system. The study was supported by NSERC, the Canada Research Chair program, and the Canada Foundation for Innovation.

*Corresponding author.
jfeng@chml.ubc.ca

[1] P. Poulin and D. A. Weitz, Phys. Rev. E **57**, 626 (1998).
[2] P. S. Drzaic, J. Appl. Phys. **60**, 2142 (1986).
[3] T. C. Lubensky, D. Pettey, N. Currier, and H. Stark, Phys. Rev. E **57**, 610 (1998).
[4] H. Stark, Phys. Rep. **351**, 387 (2001).
[5] O. Mondain-Monval, J. C. Dedieu, T. Gulik-Krzywicki, and P. Poulin, Eur. Phys. J. B **12**, 167 (1999).
[6] Y. Gu and N. L. Abbott, Phys. Rev. Lett. **85**, 4719 (2000).
[7] J. J. Feng and C. Zhou, J. Colloid Interface Sci. **269**, 72 (2004).
[8] C. Völtz, Y. Maeda, Y. Tabe, and H. Yokoyama, Phys. Rev. Lett. **97**, 227801 (2006).
[9] J. C. Loudet, Liq. Cryst. Today **14**, 1 (2005).
[10] H. Stark and D. Ventzki, Europhys. Lett. **57**, 60 (2002).
[11] M. Yoneya, J.-I. Fukuda, H. Yokoyama, and H. Stark, Mol. Cryst. Liq. Cryst. **435**, 75 (2005).
[12] C. Zhou, P. Yue, and J. J. Feng, J. Fluid Mech. **593**, 385 (2007).
[13] H. Stark, Phys. Rev. E **66**, 032701 (2002).
[14] O. D. Lavrentovich and V. M. Pergamenshchik, Phys. Rev. Lett. **73**, 979 (1994).
[15] O. D. Lavrentovich, V. G. Nazarenko, V. V. Sergan, and G. Durand, Phys. Rev. A **45**, R6969 (1992).
[16] M. Kleman and O. D. Laverntovich, *Soft Matter Physics* (Springer, New York, 2003).
[17] R. Oldenbourg, Nature (London) **381**, 811 (1996).
[18] J. Wu and P. T. Mather, Macromolecules **38**, 7343 (2005).
[19] H. Kasten and G. Strobl, J. Chem. Phys. **103**, 6768 (1995).
[20] M. G. J. Gannon and T. E. Faber, Philos. Mag. A **37**, 117 (1978).
[21] C. Zhou, P. Yue, J. J. Feng, C. Liu, and J. Shen, Phys. Fluids **19**, 041703 (2007).
[22] R. W. Ruhwandl and E. M. Terentjev, Phys. Rev. E **56**, 5561 (1997).
[23] S. Grollau, N. L. Abbott, and J. J. de Pablo, Phys. Rev. E **67**, 011702 (2003).